Journal of Thermal Analysis and Calorimetry, 2005

7013-z

STUDIES ON TRANSITION METAL MUREXIDE COMPLEXES

M. S. Masoud[1], *T. S. Kassem*[1], *M. A. Shaker*[2] *and A. E. Ali*[2*]

[1]Chemistry Department, Faculty of Science, Alexandria University, Alexandria, Egypt
[2]Physics & Chemistry Department, Faculty of Education, Damanhour, Alexandria University, Egypt

Iron, cobalt, nickel, copper, zinc, cadmium and mercury murexide complexes have been prepared and characterized. The thermal properties of these complexes are studied deeply by DTA technique where their thermal peaks are explained. The multi-stages thermal decomposition mechanism is proposed. The thermodynamic parameters of the decomposition steps are calculated. The entropy change values for all complexes are of the same magnitude and all transition states of the thermal reactions are more ordered than the reactants. The thermal reactions proceed in complicated mechanisms. The fractions appeared in the calculated orders of the thermal reactions confirmed that these reactions proceeded via complex mechanisms.

Keywords: DTA, murexide complexes of Fe, Co, Ni, Cu, Zn, Cd, Hg, thermal stability

Introduction

Murexide, a reddish purple compound has the structure shown in Fig. 1. It has received much interest because of its application in chemical analysis and spectrophotometric fields [1, 2]. It is considered as the ammonium salt of purpuric acid and named as ammonium 2,6-dioxo-5-(2,4,6-trioxo-tetrahydro-pyrimidine-5-ylidene amino)-1,2,3,6-tetrahydro-pyrimidine-4-olate. It serves as a metal ion indicator, commonly used in conventional EDTA titrations. It is also used as a chromogenic reagent for conventional spectrophotometric determination of some metals [2]. This indicator has a low potential in the literature and few studies such as surface properties [1], stability constants of its complexes [3, 4] and complex formation kinetics [5] were examined. No physico-chemical properties as well as proposed structures for these complexes were carried out. So, this paper is intended to give spotlight on the structure and thermal properties of some transition metal-murexide complexes. Transition metal complexes are of special interest in industry, medicine and biology and have many applications in thermochromism, antioxidation, vulcanization acceleration, protecting paintings, catalysis and anti-bacteriology. So far, solid-state reactions such as thermal isomerization, conformational changes, polymorphic transformations, thermal phase transitions and thermochromism have a scientific impact for coordination compounds. Our research group has reported a series of articles concerning with the thermal properties of different transition metal complexes with pyrimidine, purine, azo, nitroso, azo-nitroso and amino alcohol

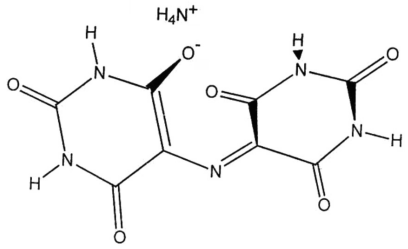

Fig. 1 Structure of murexide

derivatives [6–20]. In a continuation of such work the subject of this article is introduced.

Experimental

Preparation of the complexes

The metal murexide complexes were prepared by mixing the molar amount of the metal (Fe, Co, Ni, Cu, Zn, Cd and Hg) chloride or sulphate dissolved in 10 mL water-ethanol mixture with the calculated amount of murexide saturated with ethanol. The mixture were refluxed for about 5 min. The complexes were precipitated, filtered and then washed several times with ethanol and dried in a desiccator over anhydrous $CaCl_2$. The melting points of the complexes are over 300°C.

Analysis of metal ion content

The complexes were digested and decomposed with aquaregia. The metal ion contents were determined by the usual complexmetric procedures [21].

* Author for correspondence: dralaaeldeen@yahoo.com

1388–6150/$20.00

Akadémiai Kiadó, Budapest, Hungary
Springer, Dordrecht, The Netherlands

Carbon, hydrogen and nitrogen analyses

The carbon, hydrogen and nitrogen analyses were done at the Micro Analytical Laboratory, Faculty of Science, Alexandria University, Egypt.

Halogen and sulphate analyses

The halogen content was determined by titration with standard $Hg(NO_3)_2$ solution using diphenyl carbazone indicator [21]. The sulphate content was determined gravimetrically as $BaSO_4$ [21]. The analytical data and colors of the prepared complexes are collected in Table 1.

IR spectra

Infrared spectra were recorded as KBr disc using Perkin Elmer Spectrophotometer model 1430 covering range of 200–4000 cm^{-1}. Calibration of the frequency readings was made with polystyrene film.

ESR spectra

ESR spectra were recorded at 100 kHz modulation and 10 G modulation amplitude on Varian E-9 Spectrophotometer. Incident power of 10 mV was used and resonance conditions were at ca 9.75 GHz (X-band) at room temperature. Spectra were obtained with an air products LTD-3-110 Heli-Trans liquid helium transfer refrigerator. The field was calibrated with a powder sample of 2,2-diphenyl pyridylhydrazone (DPPH) g=2.0037 [22].

UV-Vis spectra

The electronic absorption spectra data were recorded by Perkin Elmer Spectrophotometer model 48 covering range of 190–900 cm^{-1}. The spectra were measured in nujol mull following the method described by Lee *et al*. [23].

Table 1 Analytical data and color of metal murexide complexes

Complex	Abbreviation	Color	% Calculated (Found)					
			M	C	H	N	Cl	S
$FeLCl_2·H_2O$	**I**	Orange	13.59	23.36	1.46	17.03	17.27	–
			(13.58)	(23.29)	(1.48)	(17.00)	(17.26)	
$Fe_2LCl_4·2H_2O$	**II**	Brown	20.09	17.27	1.44	12.59	25.54	–
			(20.08)	(17.28)	(1.50)	(12.59)	(25.58)	
$CoLCl·2H_2O$	**III**	Yellow	14.83	17.27	2.02	17.65	8.95	–
			(14.80)	(17.29)	(2.08)	(17.60)	(8.98)	
$Co_2LCl_3·3H_2O$	**IV**	Brown	21.64	24.20	1.84	12.85	19.56	–
			(21.70)	(24.20)	(1.80)	(12.79)	(14.54)	
$NiLCl·2H_2O$	**V**	Yellow	14.81	17.63	2.02	17.66	8.96	–
			(14.80)	(17.65)	(2.03)	(17.68)	(8.85)	
$Ni_2LCl_3·3H_2O$	**VI**	Olive-green	21.58	17.64	1.84	12.87	19.57	–
			(21.56)	(17.64)	(1.80)	(12.84)	(19.57)	
$CuLCl·2H_2O$	**VII**	Orange	15.84	23.93	1.99	17.45	8.85	–
			(15.86)	(23.96)	(1.99)	(17.45)	(8.84)	
$Cu_2LCl_3·3H_2O$	**VIII**	Brown	22.95	17.34	1.81	12.64	19.23	–
			(22.96)	(17.33)	(1.80)	(12.63)	(19.22)	
$Zn_2L_2SO_4·4H_2O$	**IX**	White	15.73	11.55	1.44	8.42	–	3.85
			(15.70)	(11.56)	(1.41)	(8.39)		(3.81)
$CdLCl·2H_2O$	**X**	White	24.97	21.33	1.78	15.55	7.89	–
			(24.97)	(21.30)	(1.75)	(15.50)	(7.86)	
$HgLCl·2H_2O$	**XI**	White	37.26	17.84	1.49	13.00	6.60	–
			(37.19)	(17.87)	(1.45)	(12.99)	(6.59)	

Magnetic susceptibility measurements

Room temperature molar magnetic susceptibilities of the complexes were measured by using an Evan balance. The measurements were calibrated against a $Hg[Co(SCN)_4]$ standard [24].

Thermal analysis

Thermogravimetric measurements and differential thermal analysis were performed on a Du Pont 9900 computerized thermal analyzer. The heating rate was 10 degree min^{-1}. A 60 mg sample was placed in a platinum crucible. Dry nitrogen was flowed over the sample at a rate 10 mL min^{-1} and a chamber cooling water flow rate was 10 L h^{-1}. The speed was 5 mm min^{-1}.

Results and discussion

Spectral and magnetic identification of murexide complexes

The structure of murexide was determined and reported [25]. In this work, the molecular structure of the murexide ligand, Fig. 2 is examined by Chem. 3D Program, and interesting data are observed. Table 2 shows some of the obtained bond lengths (Å) and bond angles (°). From Table 2, the C(23)-O(4) bond has the highest bond length value, 1.259 Å, among the other C–O bonds as this bond is more single than the others. Also, the bond angles in most cases shifted from those of tetrahedral (109.5) or trigonal planar (120) angles due to the interaction between the lone pair electrons of the heteroatoms.

The IR spectral data of the murexide ligand and its complexes are collected in Table 3. Murexide compound has various potential donor sites. All complexes show bands at 3500–3400, 750–730 and 600 cm^{-1} characteristics of stretching, rocking and waging modes of coordinated H_2O molecules. Murexide exhibits bands at 3264, 3244 cm^{-1} which are due to N–H vibration modes. The ligand gave strong splitted carbonyl bands at 1695 and 1670 cm^{-1} corresponding to the ν C=O of the amide and the band at 1653 cm^{-1} is due to the C=N vibration. The N–H and C=O bands are shifted on complexation. Murexide presumably coordinates through ring nitrogen with appreciable shifts. However, the observed

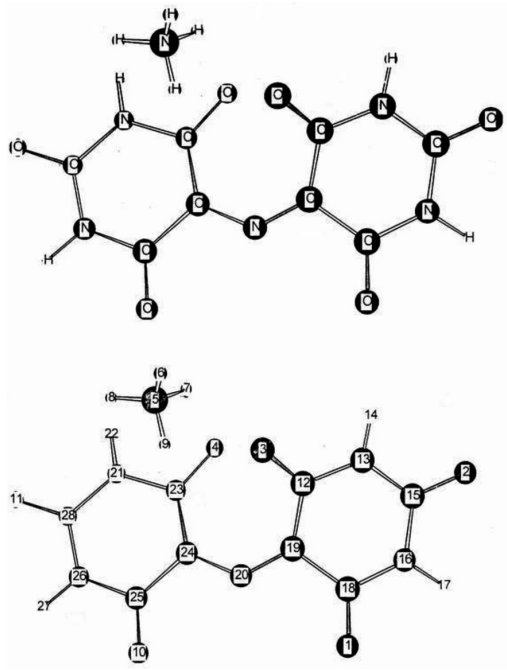

Fig. 2 The postulated structure of murexide

Table 2 The calculated lengths and angles for some murexide bonds

O(1)-C(18)	1.237	C(19)-N(20)	1.309	O(3)-C(12)-N(13)	117.193	H(22)-N(21)-C(23)	118.344
O(2)-C(15)	1.249	N(20)-C(24)	1.345	O(3)-C(12)-C(19)	124.348	O(4)-C(23)-N(21)	114.796
O(3)-C(12)	1.254	N(21)-C(23)	1.411	C(12)-N(13)-C(15)	122.560	O(4)-C(23)-C(24)	125.786
O(4)-C(23)	1.259	N(21)-C(28)	1.413	C(12)-N(13)-H(14)	120.232	N(20)-C(24)-C(23)	126.130
O(10)-C(25)	1.239	N(21)-H(22)	0.998	H(14)-N(13)-C(15)	117.052	C(23)-C(24)-C(25)	118.274
O(11)-C(28)	1.252	C(23)-C(24)	1.451	C(15)-N(16)-C(18)	123.546	O(10)-C(25)-C(24)	126.602
C(12)-N(13)	2.822	C(24)-C(25)	1.483	O(2)-C(15)-N(13)	120.119	O(10)-C(25)-N(26)	115.859
C(12)-C(19)	1.483	C(25)-N(26)	1.415	N(13)-C(15)-N(16)	118.089	C(25)-N(26)-C(28)	123.899
N(13)-C(15)	1.410	N(26)-C(28)	1.390	C(15)-N(16)-H(17)	117.267	H(27)-N(26)-C(28)	117.356
N(13)-H(14)	0.996	N(26)-H(27)	0.998	O(1)-C(18)-N(16)	117.814	O(11)-C(28)-N(26)	122.259
C(15)-N(16)	1.397	N(5)-H(6)	1.016	N(16)-C(18)-C(19)	116.235	H(6)-N(5)-H(8)	111.273
N(16)-C(18)	1.408	N(5)-H(7)	1.042	C(12)-C(19)-C(18)	115.071	H(6)-N(5)-H(9)	109.613
N(16)-H(17)	0.997	N(5)-H(8)	1.017	C(12)-C(19)-N(20)	129.118	H(7)-N(5)-H(8)	110.544
C(18)-C(19)	1.500	N(5)-H(9)	1.033	C(19)-N(20)-C(24)	131.257	H(8)-N(5)-H(9)	110.476

Table 3 Fundamental infrared bands (cm^{-1}) of murexide and its complexes

Compound	νN–H	νC=O	νC=N	νC–N	νM–O	νM–N	νM–Cl	νM–S
Murexide	3264	1729	1653	1462				
	3244	1690						
I	3295	1680	1653	1415	564	232	340	
II	3197	1659	1653	1400	536	234	344	
III	3197	1685	1653	1390	590	268	400	
IV	3195	1700	1653	1399	547	266	415	
V	3200	1705	1653	1401	522	231	431	
VI	3282	1699	1653	1425	515	299	411	
VII	3215	1688	1653	1423	437	390	399	
VIII	3166	1711	1653	1399	408	369	366	
IX	3199	1687	1653	1403	407	313		369
X	3189	1645	1653	1425	409	299	423	
XI	2990	1703	1653	1433	550	287	409	

shifts for the C=O band of the ligand on complexation indicate that it is involved in the structural configuration of the complexes. The band corresponding to νC–N (amide) in the free ligand, at 1462 cm^{-1} is shifted due to its involvement in the complexation. This indicates the donating nature of the N atom because of its resonance stabilization. The presence of both ν_{NH} and $\nu_{C=O}$ bands in the spectra of the murexide complexes and the disappearance of new bands assigned for ν_{OH} are strong evidences that no tautomerization of the NH groups with the adjacent carbonyls takes place before complexation. The complexes gave new IR bands in the ranges of 407–590 cm^{-1} corresponding to νM–O, 231–390 cm^{-1} corresponding to νM–N, 340–431 cm^{-1}corresponding to νM–Cl and at 369 cm^{-1} corresponding to νM–S.

The Nujol mull electronic absorption spectra of the separated solid murexide complexes gathered with that of effective magnetic moment values (Table 4) indicated the octahedral geometry of all complexes [26]. The magnetic moment of the iron complexes (**I, II**) at room temperature, 2.03 BM, is comparable to the low spin iron (**III**) systems with a characteristic configuration (^2T_2g ground state) [27].

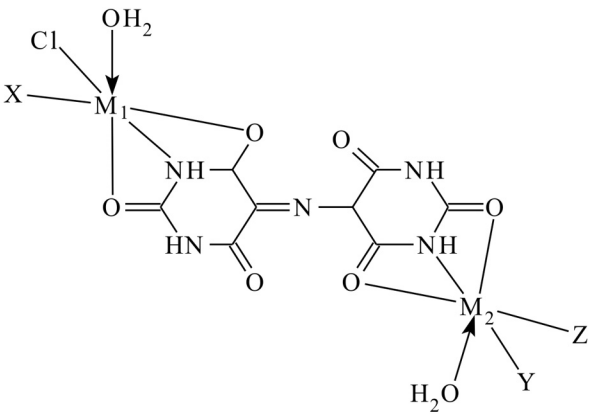

Fig. 3 The structures of all murexide complexes except **IX** where Complex **I** when there is no M_2 and M_1=Fe, X=Cl. Complexes **III**, **V**, **VII**, **X** and **XI** when there is no M_2, X=H_2O and M_1=Co, Ni, Cu and Cd , respectively. Complex **II** M_1= M_2=Fe and X=Y=Z=Cl. Complexes **IV**, **VI** and **VIII** when, X=H2O, Y=Z=Cl and M1=M2=Co, Ni and Cu, respectively

Table 4 Electronic spectral and effective magnetic moment values at 298 K for the complexes

Complex	λ_{max}/nm	μ^{eff}/BM
I	352, 550	2.03
II	352, 550	2.03
III	696(sh), 587(sh), 413(s), 312(s)	5.21
IV	696(sh), 587(sh), 413(s), 312(s)	5.21
V	853(sh), 743(w.b), 416(s), 286(s), 262(sh)	2.15
VI	853(sh), 743(w.b), 416(s), 286(s), 262(sh)	2.15
VII	683(v.b), 423(sh), 409(s), 355(w), 313(s)	2.50
VIII	683(v.b),423(sh),409(s),355(w),313(s)	2.54

The electronic absorption spectra gave the spectra of the low spin O_h iron (**III**) complexes where two spectral bands are observed at 352 and 550 nm, due to $L \rightarrow M$ charge transfer transitions. Based on the elemental analyses, spectral and magnetic measurements the structure of the murexide complexes can be proposed to be as shown in Fig. 3 where murexide acts as a tridentate monobasic ligand and the chloride ion behaves as a strong nucleophile during complexation.

ESR of copper complexes

It is possible to measure the covalent bond character α^2, where α is the coefficient of the ground state of d_{x2-y2} orbital, from the expression [28–33]:

$$\alpha^2=\frac{A_{11}}{0.036}+(g_{11}-2.0023)+\frac{3}{7}(g_{\perp}-2.0023)+0.04$$

A_{11} is the parallel coupling constant (cm^{-1}). The α^2 value for Cu(II) complexes with tetragonal distortion lies in the range of 0.63–0.84 for nitrogen donor ligands [34] and 0.84–0.94 for oxygen donor ligands [35]. Axial ligands cause changes in equatorial bond length and hence g and A values [36]. Bonding between ligands and Cu(II) ion occurs through the 4s and 4p orbitals of the Cu(II) ion with the ligand orbitals. The presence of apical ligands introduces 4s character in the ground state which decreases the contact hyperfine interaction. Therefore, if the 4s character in the ground state is known, it is possible to know the axial field strength in the presence of small percentage of 4s character in the ground state, the fraction of the 3d character in the Cu(II) 3d–4s ground state, f^2 , can be determined from the following equation [33]:

$$\alpha^2 f^2=\frac{7}{4}\left[\frac{A_{11}}{0.036}-\frac{A}{0.36}+\frac{2}{3}g_{11}-\frac{5}{21}g_{\perp}-\frac{6}{7}\right]$$

The room temperature polycrystalline X-band ESR spectral pattern of the Cu-murexide complexes (**VII, VIII**) gave similar pattern (Table 5). Both are of anisotropic nature. The spectral analysis of these complexes gave two values of g_{11} (2.11, 2.23) and of $g_{\perp}$ (2.03, 2.05) for both complexes, respectively. The calculated $\langle g \rangle$ values $=(g_{11}+2g_{\perp})/3$ are 2.06 and 2.11, respectively. The lowest g value was found to be more than 2.00, consequently, the tetragonal distorted symmetry associated with d_{x2-y2} ground state rather than dz^2 ground state is suggested [37]. The A^{11} values for the two complexes were 185 and 188, indicating the probability of the pseudo O_h structure around Cu ion in the two complexes; where the value of $A_{11}>100$. The calculated α^2 and f^2 values (Table 5) indicated the stronger axial field in the two complexes. From the values of α^2 one can say that the metal–ligand bond in complex **VII** is less covalent than that of complex **VIII**.

Thermal analysis

The compositions of the complexes were confirmed by DTA and TG. The thermal pattern of the decomposition steps of the investigated complexes showed that M-ligand bonds dissociated after removal of small molecules. At the beginning of the DTA-curves of the complexes there is a clearly manifested endothermic effect (above 100°C), which is due to the hygroscopic moisture released. The amount of this mass loss, determined also by Karl Fisher analysis, is correlated with the intensity of these endothermic effects and with the respective decreases in the mass. On heating the complexes the decomposition step in all cases corresponds to the loss of molecules of the ligands, which is in agreement with the compositions in Table 6. The exothermal effect (300–500°C) dominates in the curves of all the complexes, resulting from the decomposition of the organic matter. A further mass loss recorded up to higher temperatures indicates the formation of thermally stable oxide. The reaction order of the thermal reactions was calculated using Kissinger approach [38]. The values of the collision factor, Z were obtained, Table 6, based on Horowitz-Metzger equation [39] by making use of the following equation:

$$Z=\frac{\Delta E}{RT_m}\beta\exp(\Delta E / RT_m^2)$$

The entropies of activation $\Delta S^{\#}$ were obtained from the following equation:

$$Z=\frac{KT_m}{h}\exp(\Delta S^{\neq} / R)$$

where R is the molar gas constant β is the rate of heating ($K\ sec^{-1}$), K is the Boltzman constant and h is Planck's constant. The activation energy, ΔE_a, of the thermal decomposition step is determined from the slope of the straight line of the $\ln \Delta T$ *vs.* $1/T$ relationship. The slope is of Arrhenius type and equals to

Table 5 ESR parameters for copper murexide

Complex	g_{11}	$g_{\perp}$	$\langle g \rangle$	G	A_{11}	$A_{\perp}$	α^2	f^2
VII	2.23	2.05	2.11	3.60	188	38	0.52	0.80
VIII	2.11	2.03	2.06	3.66	185	18.5	0.67	0.98

Table 6 Thermodynamic parameters of murexide complexes

Complex	Type	T_m/°C	n	S	ΔE/kcal mol^{-1}	α_m	β	Z	$\Delta S^{\#}$/J K^{-1} mol^{-1}	$\Delta H^{\#}$/kcal mol^{-1}
I	Endo	134	1.95	3.50	28.00	1.84	2.14	59.68	–51.61	29.21
	Endo	298	1.35	0.98	33.00	2.15	2.34	79.43	–50.53	28.55
	Exo	403	0.65	0.10	50.00	3.35	1.06	86.26	–51.15	–27.98
II	Endo	105	0.73	0.63	79.23	3.17	1.69	30.04	–49.87	31.33
	Endo	300	0.87	0.48	38.20	2.55	1.59	40.18	–53.04	32.72
	Exo	430	0.87	0.47	79.20	2.60	1.59	31.08	–49.93	–31.89
III	Endo	202	1.14	0.82	87.44	2.15	2.25	179.18	–50.09	31.51
	Exo	428	1.14	0.82	41.81	2.19	2.25	78.63	–51.68	–32.52
IV	Endo	149	0.84	0.44	20.34	2.47	1.60	33.63	–52.94	26.71
	Exo	453	0.84	0.44	62.50	2.43	1.60	112.27	–50.53	–25.50
V	Endo	150	2.35	3.50	18.00	1.83	3.14	62.68	–51.55	24.21
	Endo	368	1.24	0.98	35.00	2.11	2.34	89.43	–50.97	25.55
	Exo	403	0.39	0.10	80.00	3.33	1.06	90.26	51.10	–27.60
VI	Endo	100	0.83	0.53	13.84	2.52	1.60	18.79	–54.45	32.68
	Endo	305	0.83	0.53	179.23	2.92	1.60	306.04	–48.87	29.33
	Endo	379	0.77	0.38	35.20	2.54	1.39	40.17	–53.04	33.72
	Exo	396	0.77	0.37	219.20	2.50	1.39	314.08	–48.93	–31.11
VII	Exo	100	1.05	0.69	17.69	2.28	2.09	46.19	–51.93	–21.82
	Endo	138	1.05	0.69	2.00	2.85	2.09	5.25	–56.28	28.49
	Exo	280	0.33	0.07	12.50	3.52	2.06	23.02	–53.94	–30.78
VIII	Exo	118	0.75	0.75	9.80	2.60	1.34	16.35	–53.98	–22.29
	Endo	149	0.93	0.93	38.50	2.34	1.85	83.29	–50.96	23.79
	Endo	368	0.95	0.95	21.20	2.36	1.90	38.91	–52.77	28.32
IX	Endo	115	1.32	1.10	41.00	2.10	2.485	88.24	–51.92	41.44
	Exo	386	1.32	1.10	164.44	2.03	2.485	288.59	–49.56	–39.84
	Endo	421	0.57	0.20	16.00	2.84	0.490	5.61	–57.70	40.61
X	Endo	162	1.21	0.92	59.00	2.12	2.347	136.41	–50.34	28.08
	Exo	421	1.21	0.92	129.00	2.04	2.347	330.62	–48.57	–27.09

$-\Delta E_a/R$. The change of entropy, $\Delta S^{\#}$, values for all complexes are given in Table 6. The negative values indicated that the activated complexes have more ordered structures than the reactants [40]. The lower values of the collision factor, Z, in most of the complexes indicated the slow nature of the reactions [41]. The degree of decomposition, α_m, was calculated and given in Table 6. Also, it seems that $\Delta S^{\#}$ values are nearly of the same magnitude suggesting a uniform decomposition pattern. The thermal decomposition of the murexide complex **I** showed three peaks at 134, 298 and 403°C with activation energies 28.00, 33.00 and 50.00 kcal mol^{-1}, respectively, and an order of reactions 1.95, 1.35 and 0.65, respectively. The latter peak is assigned to the Fe_2O_3. The first peak is due to the dehydration reaction of probably adsorbed water. Its decomposition begins at 134°C and proceeds in three stages involving a loss in mass. The stages probably consist of a number of unidentifiable processes. The dehydration of the iron complex is suggested in stage 1. The processes occurring in the endothermic first stage of the decomposition partly coincide with those of the second stage, so it is difficult to determine precisely the corresponding temperature ranges. The total thermal effect of the second stage is endothermic (an intense endo peak). Above 403°C the next stage of the decomposition (stage 3) of the sample proceeds involving a stepwise loss of its mass. The thermal decomposition of complex **II** is similar to that observed for the complex **I**, but the processes are preceded by dehydration at 105°C (stage 1). It showed also three peaks at 105, 300 and 430°C with activation energies 79.23, 38.20 and 79.20 kcal mol^{-1}, respectively, and an order of reactions 0.73, 0.87 and 0.87, respectively. The analysis of the mass spectra of the gaseous products of complex **II** decomposition confirmed that water molecules are released in the first stage of decomposition. In the temperature range

200–380°C, the anhydrous salt from stage 1 decomposes rapidly (the second stage), and then more slowly between 380 and 450°C (the third stage). The processes which take place in the second and third stages are endothermic and exothermic, respectively. The final product of decomposition is also ferric oxide. At temperatures exceeding 350°C the decomposition of the sample is firstly slow and then at over 800°C, its rate increases, resulting in the formation and stepwise evaporation of iron oxide. In the thermal curves of the octahedral murexide complex **III** two main stages of decomposition can be distinguished, connected with continuous mass loss and strong exothermic effects. Its DTA curve of these exhibits two peaks one is endothermic and the other is exothermic in the temperature range 202–428°C, Table 6. The presence of CoO and CoCl was confirmed in the sinter obtained at about 300°C. Above 500°C the mass of the sample does not change. The main gaseous products of the decomposition of the complexes under study are CO_2, small amounts of H_2O and trace amounts of HCl. A careful examination of the thermal decomposition curves of murexide complex **IV** reveals that decomposition proceeds via two steps. The complex is stable up to 115°C and undergoes a violent endothermic decomposition in the temperature range 115–150°C. Mass loss calculations suggest the loss of a water molecule. A color change from brown to deep blue was also observed during decomposition. The order of the decomposition reaction was 0.84 and the ΔE_a value was calculated as 20.34 kcal mol^{-1}. The intermediate formed is stable up to 220°C and decomposes in one step to give CoO as the end product at 453°C in an exothermic step. Complex **V** decomposes in three stages. The first stage corresponds to dehydration in the temperature range 100–150°C. Thermal dehydration is first order with energy of activation of 18.0 kcal mol^{-1}. In the second stage, the anhydrous complex undergoes a strong endothermic decomposition between 150 and 368°C to produce a stable solid moiety. A large mass loss was observed in this decomposition stage with a sharp color change from pale-blue to dark blue. This step is endothermic with a ΔE_a value of 35.0 kcal mol^{-1}. The third stage corresponds to the decomposition of the intermediate to yield NiO as the final decomposition product. Complex **VI** begins to lose mass around 100°C and up to 300°C. This is the dehydration stage in which two water molecules are eliminated. No stable intermediate is formed between the first and second stages as the second stage starts at 305°C. Around 300°C, a sharp decrease in mass is noted and the subsequent slow mass loss occurs until 379°C. The last stage, that starts around 396°C suggests the formation of NiO residue, which is stable even above 800°C. The thermal mode of decomposition of the murexide complex **VII** indicates that it is thermally stable up to 100°C. The thermal decomposition appears to take place in two stages, one is endothermic and the other is exothermic at 138 and 280°C, respectively. The final decomposition product was estimated as CuO. TG of the complex **VIII** starts to decompose around 118°C. This stage continues until 149°C and one water molecule is eliminated. The main degradation step starts around 368°C in the last step. Residue, in this case, is again $CuCl_2$. Thermal dehydration of complex **IX** apparently occurs in three steps. The ΔE_a and n values were found to be 41.00, 164.40 and 16.00 kcal mol^{-1} and 1.32, 1.32 and 0.57, respectively. The mass loss at 115°C accounts for the endothermic elimination of a water molecule and the formation of a stable solid intermediate. The decomposition process is about first order with a ΔE_a value of 41.00 kcal mol^{-1}. The major decomposition is observed in the temperature range 386–421°C with a mass loss to yield ZnO. The order of dehydration of the complex was found to be 1.32 while the order of decomposition was 0.57. The energies of activation of dehydration were somewhat lower than that of the second stage of decomposition. The DTA curve of the complex **X** shows two peaks, endothermic and exothermic corresponding to the first and last step of the TG curves. First step in the decomposition of the complex at 162°C is accompanied by endothermic effect in the DTA curves with the evolution of one molecule of HCl moiety from the complex. Last step in the thermal decomposition involves the decomposition of intermediates and oxidation of metal by atmospheric oxygen.

References

1 W. Grochala and J. Bukowska, Vibrational Spectroscopy, 17 (1998) 145.
2 K. Grudpan, J. Jakmunee, Y. Vaneesorn, S. Watanesk, U. A. Maung and P. Sooksamiti, Talanta, 46 (1998) 1245.
3 T. K. Khan and P. B. Gupta, Talanta, 44 (1997) 2087.
4 Y. T. Nakamura, H. Shata, M. Minao, H. Ogawa, N. Sekiguchi, M. Murata and S. Homma, Lebensmittel Wissenschaft und Technologie, 27 (1994) 115.
5 J. Ghasemi and M. Shamsipur, Polyhedron, 15 (1996) 923.
6 M. S. Masoud, E. M. Soliman, A. E. El-Kholy and E. A. Khalil, Thermochim. Acta, 1 (1988) 153.
7 M. S. Masoud and Z. M. Zaki, Trans. Met. Chem., 13 (1988) 321.
8 M. S. Masoud, E. M. Soliman and A. M. Heiba, Transition Met. Chem., 14 (1989) 175.
9 M. S. Masoud and S. A. Abou El-Enein, Thermochim. Acta, 140 (1989) 365.
10 M. S. Masoud, S. A. Abou El-Enein and E. El-Shereafy, J. Therm. Anal. Cal., 37 (1991) 365.
11 M. S. Masoud and S. S. Haggag, Thermochim. Acta, 196 (1992) 221.

12 M. S. Masoud, S. A. Abou El-Enein and O. F. Hafez, J. Thermal Anal., 38 (1992) 1365.
13 M. S. Masoud, O. H. Abd El-Hamid and Z. M. Zaki, Transition Met. Chem., 19 (1994) 21.
14 M. S. Masoud, A. A. Hasanein, A. K. Ghonaim, E. A. Khalil and A. A. Mahmoud, Z. Phys. Chem., 209 (1999) 223.
15 M. S. Masoud, E. A. Khalil, A. A. Ibrahim and A. A. Marghany, Z. Phys. Chem., 211 (1999) 13.
16 M. S. Masoud, A. K. Ghonaim, R. H. Ahmed, A. A. Mahmoud and A. E. Ali, Z. Phys. Chemie., 215 (2001) 53.
17 M. S. Masoud, A. K. Ghonaim, S. A. Abou El-Enein and A. A. Mahmoud, J. Coord. Chem., 55 (2003) 79.
18 M. S. Masoud, A. A. Soayed, A. E. Ali and O. K. Sharsherh, J. Coord. Chem., 56 (2003) 725.
19 M. S. Masoud, S. A. Abou El-Enein and N. A. Obeid, Z. Phys. Chem., 215 (2001) 867.
20 M. S. Masoud, S. A. Abou El-Enein, H. A. Motaweh and A. E. Ali, J. Therm. Anal. Cal., 74 (2003) 1.
21 A. I. Vogel, A Text Book of Quantitative Inorganic Analysis, Fourth ed., Longmann, London, 452 (1978) 116.
22 P. H. Lee, E. Griswold and J. Kleinberg, Inorg. Chem., 3 (1964) 1278.
23 D. Reinen and G. Friebel, Inorg. Chem., 23 (1984) 791.
24 N. B. Figgs and J. Lewis, Modern Coordination Chemistry, Interscience, New York, p. 403, (1967).
25 R. L. Martin, A. H. White and A. C. Willis, J. Chem. Soc., Dalton, Trans., 1336, (1977).
26 D. K. Johonson, H. J. Stklosa, J. R. Wasson and W. L. Seebach, J. Inorg. Nucl. Chem., 37 (1975) 1397.
27 B. F. Little and G. J. Long, Inorg. Chem., 17 (1978) 3401.
28 D. B. Brown, J. W. Hall, H. M. Helis, E. G. Walton, D. J. Hodgson and W. E. Halfield, Inorg. Chem., 16 (1977) 2675.
29 W. Levason and C. M. MacAulife, Inorg. Chim. Acta, 14 (1975) 127.
30 S. C. Bhtia, J. M. Bindlish, A. R. Saini and P. C. Jain, J. Chem. Soc., Dalton Trans., 1773, (1981).
31 I. Saski, D. Pujol, A. Gauderner, A. Chiaroni and C. Riche, Polyhedron, 6 (1987) 2103.
32 R. K. Parasher, R. C. Sharma, A. Kumar and G. Hohan, Inorg. Chim. Acta, 72 (1988) 201.
33 H. A. Kuska, M. T. Rogers and R. E. Drullinger, J. Phys. Chem., 71 (1967) 109.
34 D. R. Lorenz, J. R. Wasson, D. K. Johonson and D. A. Thorpe, J. Inorg. Nucl. Chem., 37 (1975) 2297.
35 D. K. Johonson, H. J. Stklosa, J. R. Wasson and W. L. Seebach, J. Inorg. Nucl. Chem., 37 (1975) 1397.
36 B. A. Stastry, S. M. Asdullah, G. Ponticelli and M. Massacesi, J. Chem. Phys., 70 (1979) 2834.
37 M. H. Sonar and A. S. R. Murty, J. Inorg. Nucl. Chem., 42 (1980) 815.
38 H. E. Kissinger, Anal. Chem., 29 (1957) 1702.
39 H. Horowitz and G. Metzger, Anal. Chem., 35 (1963) 1464.
40 K. G. Mallikarjum and A. K. Bansal, Thermochim. Acta, 206 (1992) 273.
41 S. S. Sawhney and A. K. Bansal, Thermochim. Acta, 66 (1983) 347.

DOI: 10.1007/s10973-005-7013-0